Article

Cell Reports

Deregulation of the Ras-Erk Signaling Axis Modulates the Enhancer Landscape

Graphical Abstract

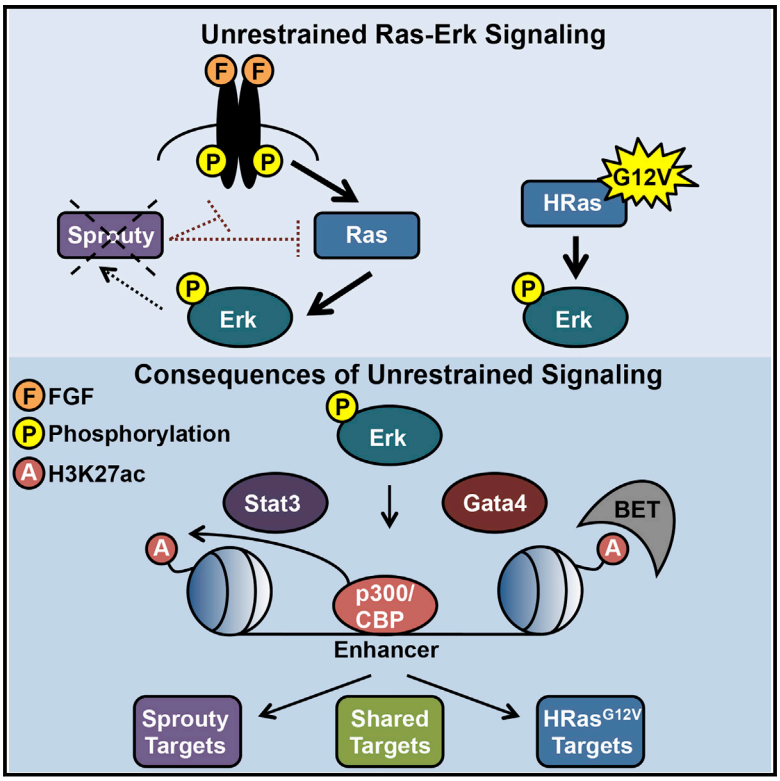

Highlights

- Unrestrained Ras-Erk signaling deregulates histone marking at active enhancers
- *Sprouty* loss and oncogenic $HRas^{G12V}$ alter distinct enhancers and target genes
- Gata4 is necessary for $HRas^{G12V}$-driven enhancer marking and target gene expression
- Prkcb and BET bromodomains are necessary for the oncogenic effects of $HRas^{G12V}$

Authors

Behnam Nabet, Pilib Ó Broin, Jaime M. Reyes, ..., James E. Bradner, Aaron A. Golden, Jonathan D. Licht

Correspondence

j-licht@northwestern.edu

In Brief

Aberrant receptor tyrosine kinase signaling mediated by oncogenic Ras or loss of *Sprouty* promotes tumorigenesis. Nabet et al. find that unrestrained receptor tyrosine signaling driven by these lesions alters distinct super-enhancers, transcription factors, and target genes. Gata4 and Prkcb are identified as mediators of the oncogenic program upon Ras transformation.

Accession Number

GSE64195

Nabet et al., 2015, Cell Reports *12*, 1300–1313
August 25, 2015
http://dx.doi.org/10.1016/j.celrep.2015.06.078

OPEN ACCESS
CellPress

Cell Reports
Article

Deregulation of the Ras-Erk Signaling Axis Modulates the Enhancer Landscape

Behnam Nabet,[1,2] Pilib Ó Broin,[3] Jaime M. Reyes,[4] Kevin Shieh,[3] Charles Y. Lin,[4] Christine M. Will,[1] Relja Popovic,[1] Teresa Ezponda,[1] James E. Bradner,[4] Aaron A. Golden,[3,5] and Jonathan D. Licht[1,*]

[1]Division of Hematology/Oncology, Northwestern University Feinberg School of Medicine, Chicago, IL 60611, USA
[2]Driskill Graduate Program in Life Sciences, Northwestern University Feinberg School of Medicine, Chicago, IL 60611, USA
[3]Department of Genetics, Albert Einstein College of Medicine, Bronx, NY 10461, USA
[4]Department of Medical Oncology, Dana-Farber Cancer Institute, Boston, MA 02115, USA
[5]Department of Mathematical Sciences, Yeshiva University, New York, NY 10033, USA
*Correspondence: j-licht@northwestern.edu
http://dx.doi.org/10.1016/j.celrep.2015.06.078

SUMMARY

Unrestrained receptor tyrosine kinase (RTK) signaling and epigenetic deregulation are root causes of tumorigenesis. We establish linkage between these processes by demonstrating that aberrant RTK signaling unleashed by oncogenic $HRas^{G12V}$ or loss of negative feedback through *Sprouty* gene deletion remodels histone modifications associated with active typical and super-enhancers. However, although both lesions disrupt the Ras-Erk axis, the expression programs, enhancer signatures, and transcription factor networks modulated upon $HRas^{G12V}$ transformation or *Sprouty* deletion are largely distinct. Oncogenic $HRas^{G12V}$ elevates histone 3 lysine 27 acetylation (H3K27ac) levels at enhancers near the transcription factor Gata4 and the kinase Prkcb, as well as their expression levels. We show that Gata4 is necessary for the aberrant gene expression and H3K27ac marking at enhancers, and Prkcb is required for the oncogenic effects of $HRas^{G12V}$-driven cells. Taken together, our findings demonstrate that dynamic reprogramming of the cellular enhancer landscape is a major effect of oncogenic RTK signaling.

INTRODUCTION

Enhancers are collections of DNA motifs that govern gene expression at long distances from transcriptional start sites, establishing cellular identity. Enhancers contain binding sites for sequence-specific transcription factors (TFs) and associated cofactors that assemble in a combinatorial manner to promote cell-type-specific gene expression patterns (Spitz and Furlong, 2012). Enhancer dysfunction contributes to disease progression and occurs through mutation of enhancer regulatory factors, such as *P300* and *CBP* in Rubinstein-Taybi syndrome, as well as through changes in the underlying enhancer DNA sequence, such as rearrangement of the IgH enhancer aberrantly activating *c-MYC* in Burkitt's lymphoma (Smith and Shilatifard, 2014). This underscores the importance of understanding how enhancers function in normal development and disease.

Histone modification signatures can be used to classify enhancers. Primed and poised enhancers are identified by the presence of histone 3 lysine 4 mono-methylation (H3K4me1) and lack of histone 3 lysine 4 tri-methylation (H3K4me3), whereas active enhancers are marked with histone 3 lysine 27 acetylation (H3K27ac) and H3K4me1 (Creyghton et al., 2010; Heintzman et al., 2007; Rada-Iglesias et al., 2011). The deposition of H3K4me1 by MLL2 and MLL3, and H3K27ac by p300 and CBP, is dynamically regulated (Brown et al., 2014; Herz et al., 2012; Kaikkonen et al., 2013; Ostuni et al., 2013; Tie et al., 2009). For example, upon activation of NF-κB signaling, primed enhancers transition to an active state by gaining H3K27ac at regions with pre-existing H3K4me1. At a subset of unmodified regions, inducible deposition of H3K4me1 and H3K27ac occurs at latent or de novo enhancers (Kaikkonen et al., 2013; Ostuni et al., 2013). Super-enhancers (SEs), which are similar to locus control regions or stretch enhancers, are an additional class of regulatory regions that contain clusters of typical enhancers (TEs) and extend over several kilobases of the genome (Smith and Shilatifard, 2014). SEs are disproportionately marked with H3K27ac, are preferentially occupied by enhancer-associated factors including bromodomain and extra-terminal domain (BET) coactivator proteins such as BRD4, and control transcriptional regulators and fate-determining genes in normal and malignant cells (Lovén et al., 2013; Whyte et al., 2013). During the inflammatory response, SEs are rapidly modified, as NF-κB directs BRD4 redistribution at SEs (Brown et al., 2014). Although controlled pathway activation triggers dynamic chromatin remodeling at enhancers, how oncogenic signaling globally remodels enhancers has not been extensively studied.

Although stimuli can elicit chromatin remodeling and TF assembly at enhancers and promoters, the rapid activation of signaling pathways precedes transcriptional responses. Receptor tyrosine kinase (RTK) signaling pathways are one example of a critical signaling network that is required for normal

development and is misregulated in disease. Fibroblast growth factor (FGF)-mediated RTK activation triggers the Ras-ERK signaling cascade, dictating whether a cell will divide, survive, migrate, or differentiate (Turner and Grose, 2010). Mutations in signaling effectors including *RAS*, *BRAF*, and *PIK3CA*, which are among the most commonly mutated genes in cancer, unleash critical RTK pathways including the Ras-ERK and PI3K-AKT signaling cascades to promote tumorigenesis (Kandoth et al., 2013; Stephen et al., 2014). RTK signaling cascades are also regulated by feedback loops that promote or limit pathway activation. *Sprouty* genes (*Spry1,2,3,4*) encode RTK feedback inhibitors required for development of the kidney, inner ear, and other organs (Basson et al., 2005; Edwin et al., 2009; Shim et al., 2005). Spry proteins primarily silence the Ras-ERK pathway while also antagonizing the PI3K-AKT and PLCγ-PKC pathways (Akbulut et al., 2010; Hacohen et al., 1998; Schutzman and Martin, 2012). Spry proteins have tumor suppressor activity, and their expression levels are commonly downregulated in cancer, leading to aberrant amplification of RTK pathways, while their re-expression inhibits malignant growth (Masoumi-Moghaddam et al., 2014). As such, it is important to understand how unrestrained RTK signaling mediated by mutant oncogenes or Spry disruption coordinates changes in gene expression to promote malignant transformation.

The Ras-ERK signaling axis in part regulates gene expression through control of activating and repressive epigenetic mechanisms. Active ERK1/2 directly binds DNA, controls RNA polymerase II, and works in concert with TFs such as ELK1 to modulate gene expression (Göke et al., 2013; Hu et al., 2009; Tee et al., 2014). ERK1/2 indirectly impinges on chromatin by controlling the activity of MSK1/2, which is responsible for histone 3 serine 10 and serine 28 phosphorylation (H3S10ph and H3S28ph), and p300 (Chen et al., 2007; Soloaga et al., 2003). The Ras-Raf axis also activates the *INK4A-ARF* locus through upregulation of the histone demethylase *JMJD3*, leading to loss of histone 3 lysine 27 tri-methylation (H3K27me3) (Agger et al., 2009; Barradas et al., 2009). These examples of the interaction between RTK signaling and chromatin modifications, and their importance in tumorigenesis, led us to investigate whether unrestrained RTK signaling driven by loss of feedback regulation or mutant oncogene expression reprograms enhancer-associated chromatin modifications. In this study, we found that chronic Ras-Erk signaling mediated by *Spry* loss leads to inappropriate gene activation, which correlates with dynamic changes in H3K27ac at SEs and TEs. Constitutive $HRas^{G12V}$, $KRas^{G12V}$, or $BRaf^{V600E}$ activation also leads to aberrant H3K27ac marking at SEs and TEs. However, the deregulated enhancers, target genes, and TF networks affected by oncogenic activation and loss of feedback regulation largely differ. Using the deregulated $HRas^{G12V}$ enhancer chromatin signature, we identified Gata4 as a key deregulated transcriptional regulator and Prkcb as a critical downstream kinase mediating the aberrant gene expression and oncogenic effects of $HRas^{G12V}$-transformed cells, respectively. Our work suggests that unrestrained RTK activation modulates gene expression and contributes to malignant transformation through enhancer deregulation.

RESULTS

Spry Loss Persistently Activates Erk Signaling and Deregulates Gene Expression

To assess the consequences of *Spry1,2,4* loss on Ras-Erk signaling and gene expression, we compared immortalized mouse embryonic fibroblasts (MEFs) with wild-type *Spry1,2,4* expression and genetically matched cells with *Spry1,2,4* knocked out. This model was created by transducing $Spry1,2,4^{flox/flox}$ MEFs with either a control adenovirus empty vector (EV) (*Spry1,2,4* wild-type MEFs, referred to as $Spry124^{fl/fl}$) or an adenovirus expressing Cre to delete *Spry1,2,4* (*Spry1,2,4* deficient MEFs, referred to as $Spry124^{-/-}$) (Akbulut et al., 2010) (Figure S1A). We found that $Spry124^{-/-}$ MEFs exhibited elevated active, phosphorylated Erk at baseline in unsynchronized and serum-starved states relative to $Spry124^{fl/fl}$ MEFs (Figure 1A). $Spry124^{-/-}$ MEFs also displayed elevated Erk activation 15–60 min after FGF treatment, which persisted for 240 min, a time point at which Erk activation returned to baseline levels in $Spry124^{fl/fl}$ MEFs. These molecular differences correlated with phenotypic characteristics of $Spry124^{-/-}$ MEFs, including more rapid proliferation in low-FGF conditions and increased cell-cycle entry in response to FGF after serum deprivation (Figures 1B and S1B). Consistent with previous data, our results indicate that *Spry* loss amplifies FGF-mediated Ras-Erk signaling (Hacohen et al., 1998; Shim et al., 2005).

To identify specific genes that may underlie the effects observed upon *Spry* loss, we performed RNA-sequencing (RNA-seq) comparing $Spry124^{fl/fl}$ and $Spry124^{-/-}$ MEFs. Given the increased baseline Erk activation in $Spry124^{-/-}$ MEFs, we first identified the differentially expressed genes in the unsynchronized states of $Spry124^{fl/fl}$ and $Spry124^{-/-}$ MEFs (Table S1). Ingenuity Pathway Analysis (IPA) revealed that these deregulated genes are involved in cancer and cardiovascular disease and in cellular movement, morphology, and growth (Figure S1C). Gene set enrichment analysis (GSEA) also revealed that these deregulated genes are associated with breast cancer, signaling pathways, and chromatin regulators including PRC2 and MLL, suggesting that epigenetic deregulation is a consequence of persistent signaling upon *Spry* loss (Figure S1D).

To examine the signal-dependent transcriptional response in these cells, we identified the FGF-responsive genes in $Spry124^{fl/fl}$ MEFs and queried how they were regulated in $Spry124^{-/-}$ MEFs. In general, FGF-induced $Spry124^{fl/fl}$ genes were elevated in $Spry124^{-/-}$ MEFs in the unsynchronized and starved states, consistent with basal pathway activation prior to FGF treatment (Figure 1C; Table S1). We subsequently identified the FGF-responsive genes that were modulated in $Spry124^{-/-}$ MEFs (Figure 1D; Table S1). By contrast, FGF-induced $Spry124^{-/-}$ genes displayed significantly elevated expression levels in all cellular states in $Spry124^{-/-}$ MEFs. However, in both analyses, FGF-repressed $Spry124^{fl/fl}$ and $Spry124^{-/-}$ genes were largely overlapping in each comparison (Figures 1C and 1D). Therefore, we focused on $Spry124^{-/-}$ target genes that displayed both elevated baseline and FGF-induced activation. Many of these deregulated factors promote cellular migration (*Itgb3, Fgf2*, *Mmp13*, and *Serpinb2)* and inflammation (*Ccl2*, *Ptpn22*, and

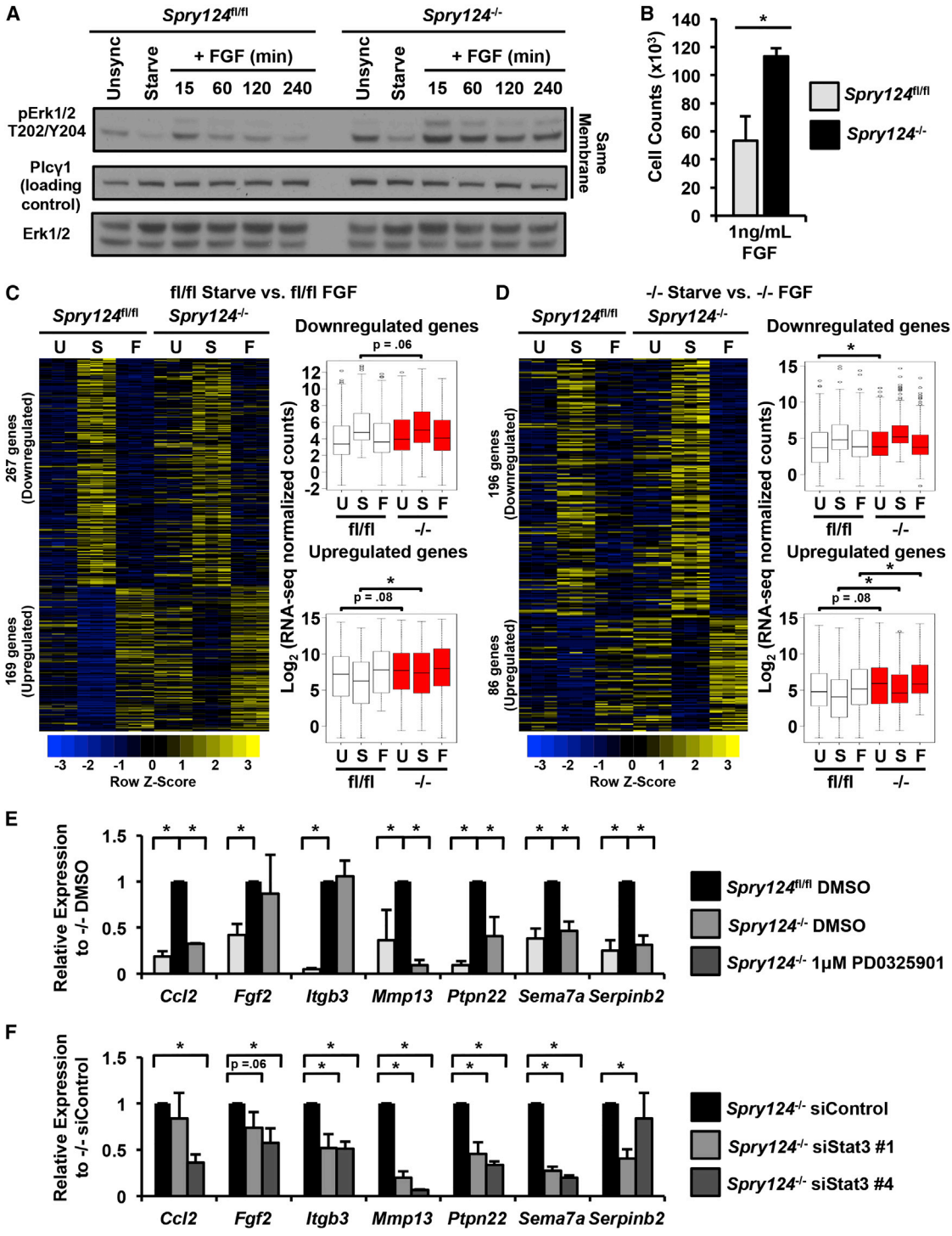

Figure 1. Chronic Erk Signaling Is Required for the Aberrant Gene Expression upon *Spry* Loss

(A) Immunoblot analysis of *Spry124*$^{fl/fl}$ and *Spry124*$^{-/-}$ MEFs that were freely growing (Unsync), serum starved (Starve), or serum starved and treated with FGF over the time course indicated.

(B) Cell counts of *Spry124*$^{fl/fl}$ and *Spry124*$^{-/-}$ MEFs cultured in the presence of FGF.

(C and D) RNA-seq analysis of *Spry124*$^{fl/fl}$ and *Spry124*$^{-/-}$ MEFs under unsynchronized (U), starved (S), and FGF-treated (F) states. Heatmaps and boxplots depict the significantly differentially expressed genes comparing *Spry124*$^{fl/fl}$ (C) and *Spry124*$^{-/-}$ (D) MEFs in starved and FGF-treated conditions.

(E) Relative mRNA levels of *Spry124*$^{-/-}$ target genes upon treatment of *Spry124*$^{-/-}$ MEFs with DMSO or PD0325901. mRNA levels of *Spry124*$^{fl/fl}$ MEFs treated with DMSO are shown as a baseline reference.

(legend continued on next page)

Sema7a). These seven *Spry124*$^{-/-}$ target genes displayed little to no activation in *Spry124*$^{fl/fl}$ MEFs and were selected as a representative panel of *Spry124*$^{-/-}$ target genes for further assessment (Figure S1E). Treatment of *Spry124*$^{-/-}$ MEFs with a MEK inhibitor, PD0325901 (Barrett et al., 2008), led to a dose-dependent reduction in Erk activation, and reduced baseline expression of five out of seven *Spry124*$^{-/-}$ target genes tested to *Spry124*$^{fl/fl}$ levels, indicating their dependence on Erk signaling (Figures 1E and S1F). We also noted that a number of *Spry124*$^{-/-}$ targets, including *Ccl2* and *Fgf2*, are Stat3 target genes (Yu et al., 2009), suggesting that Stat3, an oncogenic TF activated by RTK signaling, may be aberrantly activated upon *Spry* loss. Accordingly, *Spry124*$^{-/-}$ MEFs displayed elevated constitutive phosphorylation of Stat3 tyrosine 705 and enhanced FGF-induced phosphorylation of Stat3 serine 727 (Figure S1G). Furthermore, Stat3 knockdown reduced the expression of all seven *Spry124*$^{-/-}$ target genes tested (Figures 1F and S1H). Collectively, these data indicate that a transcriptional program activated by *Spry* loss is driven by persistent Erk signaling and requires Stat3 activation.

Spry Loss Deregulates Chromatin Marking at Enhancers

To explore the consequences of persistent Erk signaling on histone modifications associated with gene activation, we performed chromatin immunoprecipitation (ChIP) followed by next-generation sequencing (ChIP-seq) for the enhancer marks, H3K4me1 and H3K27ac, and the active promoter mark, H3K4me3. To identify TEs and SEs in each dataset, enhancer regions were rank ordered based on the extent of H3K27ac enrichment (Lovén et al., 2013) (Figure S2A; Table S4). The median length and signal of H3K27ac at SEs is an order of magnitude greater than TEs. SEs accounted for 14%–21% of the H3K27ac signal (Figure S2B). Comparing *Spry124*$^{fl/fl}$ and *Spry124*$^{-/-}$ MEFs in unsynchronized, starved, or FGF-treated states, we observed significant gains and losses in H3K27ac at TEs and SEs (Figures 2A and S2C). The absolute change in H3K27ac signal between *Spry124*$^{fl/fl}$ and *Spry124*$^{-/-}$ MEFs was significantly greater at SEs than TEs (Figure 2B). Furthermore, gain or loss of an SE in *Spry124*$^{-/-}$ MEFs had a significantly greater effect on gene expression than did changes at TEs (Figure 2C). This suggests that chromatin changes at SEs mediated the transcriptional effects of unrestrained signaling upon *Spry* loss. We therefore focused on the SE signatures and examined the sequences at gained *Spry124*$^{-/-}$ SEs. This analysis revealed significant enrichment of binding sites for TFs such as NFIA/B ($p < 10^{-6}$), ETS family members such as ETV1 ($p < 0.001$), NF-κB2 ($p < 0.005$), and STAT3 ($p < 0.005$) in *Spry124*$^{-/-}$ MEFs (Figure 2D; Table S6). This finding is consistent with the aberrant activation of NF-κB and Stat3 in *Spry124*$^{-/-}$ MEFs, the requirement of Stat3 for expression *Spry124*$^{-/-}$ targets, and the known role of NF-κB and STAT factors in enhancer remodeling (Brown et al., 2014; Ostuni et al., 2013) (Figures 1F, S1G, and S2D).

We also examined whether enhancers were remodeled after FGF treatment (Figure 2A). Hierarchical clustering analyses of the SE signatures highlighted the high reproducibility among the biological replicates and demonstrated that the *Spry124*$^{fl/fl}$ and *Spry124*$^{-/-}$ SE signatures clustered separately with moderate changes across each cellular state (Figure 2E; Table S3). Baseline changes in SEs were largely maintained upon starvation and FGF treatment. For example, the oncogenic *Hoxa* cluster scored as an SE and displayed elevated H3K27ac enrichment in the presence or absence of FGF in *Spry124*$^{-/-}$ MEFs, which correlated with elevated expression of *Hoxa3-5* and H3K4me3 promoter enrichment (Figure 2F; Table S1). Similarly, a broad region upstream of the inflammatory cytokine, *Ccl2*, displayed elevated H3K27ac enrichment in *Spry124*$^{-/-}$ MEFs and reached SE levels in most conditions, correlating with elevated expression of *Ccl2* and the presence of H3K4me3 at its promoter (Figures S1E and S2E). Although SEs were largely unresponsive to FGF treatment, there were significant changes at TEs associated with *Spry124*$^{-/-}$ target genes (Figures 2A and S2A). For example, in *Spry124*$^{-/-}$ MEFs, a TE downstream of *Sema7a* exhibited increased H3K27ac in the unsynchronized and starved states, which was further elevated upon FGF treatment. Again, these differences correlated with elevated *Sema7a* expression and increased H3K4me3 at its promoter (Figures S1E and S2E). These data indicate that *Spry* loss leads to significant changes in H3K27ac at critical enhancers in all cellular states.

Abrogating Erk Signaling Diminishes H3K27ac at Enhancers, while Oncogenic Ras and Raf Promote H3K27ac at Enhancers

Next, we tested whether chromatin modifications at SEs and TEs were maintained after inhibiting aberrant Erk signaling. Treatment of *Spry124*$^{-/-}$ MEFs with PD0325901 significantly reduced H3K27ac levels at sites associated with *Ccl2, Sema7a*, and *Mmp13* and decreased expression of these genes (Figures 1E and 3A). However, H3K4me1 was maintained at these sites, indicating that Erk signaling activates these primed enhancers by directing the deposition of H3K27ac (Figure 3B). Since Erk signaling was required to maintain H3K27ac, we predicted that BET bromodomain proteins and p300/CBP, which recognize and deposit H3K27ac, respectively, are necessary for the aberrant activation of *Spry124*$^{-/-}$ target genes. Accordingly, treatment of *Spry124*$^{-/-}$ MEFs with the BET bromodomain inhibitor, JQ1, which prevents association of BRD4 with TEs and SEs of oncogenes to inhibit cancer cell growth (Filippakopoulos et al., 2010; Lovén et al., 2013), significantly reduced the elevated baseline and FGF-mediated expression of all seven *Spry124*$^{-/-}$ target genes tested to *Spry124*$^{fl/fl}$ levels (Figure S3A). In addition, treatment of *Spry124*$^{-/-}$ MEFs with the p300/CBP inhibitor, C646 (Bowers et al., 2010), significantly reduced the expression of four out of seven *Spry124*$^{-/-}$ target genes tested upon serum deprivation and significantly diminished FGF-mediated gene activation to *Spry124*$^{fl/fl}$ levels (Figure S3B). Collectively, our

(F) Relative mRNA levels of *Spry124*$^{-/-}$ target genes upon treatment of *Spry124*$^{-/-}$ MEFs with control or *Stat3* small interfering RNAs (siRNAs).

n = 3 for (A)–(F). In (A), a representative biological replicate is shown. In (B), (E), and (F), the values depict the mean + SD of biological replicates. In (C) and (D), each replicate per condition is shown in the heatmap, and the replicates are averaged in the boxplots. The p values were calculated by a two-tailed t test in (B), (E), and (F) and Wilcoxon rank sum test in (C) and (D); *$p < 0.05$.

A

Gained/Lost Enhancers Comparing fl/fl vs. -/-				
Culture Condition	-/- Gained TE	-/- Gained SE	-/- Lost TE	-/- Lost SE
Unsync	6819	102	750	44
Starve	9805	116	580	53
FGF	7183	210	1069	40

Gained/Lost Enhancers Comparing Starve vs. FGF				
Cell Line	FGF Gained TE	FGF Gained SE	FGF Lost TE	FGF Lost SE
fl/fl	1370	22	1000	12
-/-	1246	25	1489	9

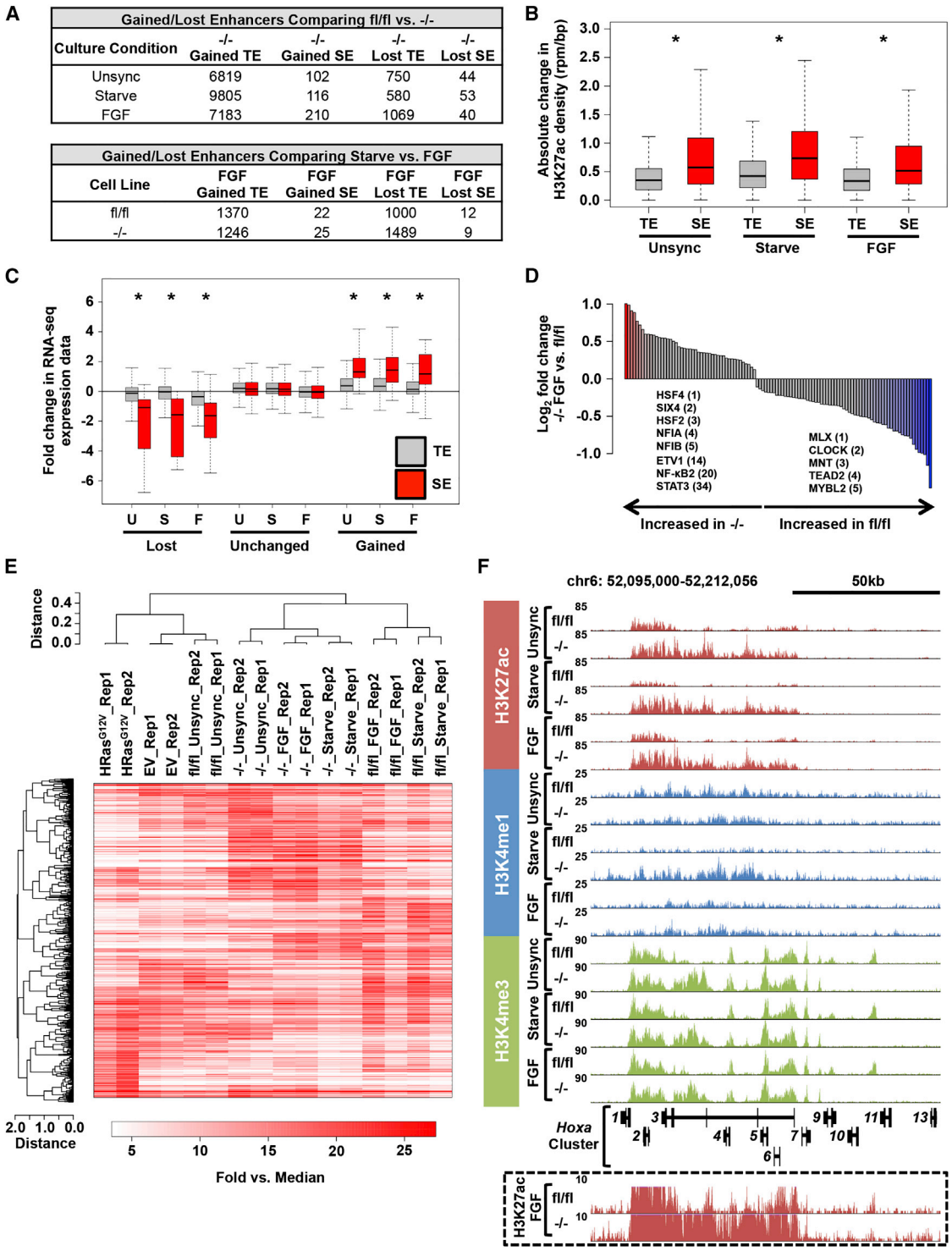

Figure 2. *Spry* Loss Globally Reprograms Enhancer-Associated Chromatin Modifications

(A) Table summarizing the number of H3K27ac defined enhancers significantly modulated between *Spry124*$^{fl/fl}$ and *Spry124*$^{-/-}$ MEFs in the indicated comparisons.

(B) Boxplot of the absolute change in H3K27ac density between *Spry124*$^{fl/fl}$ and *Spry124*$^{-/-}$ MEFs at TEs and SEs.

(C) Boxplot of RNA-seq expression for genes proximal to TEs and SEs that were gained, unchanged, or lost in *Spry124*$^{-/-}$ MEFs upon comparison between *Spry124*$^{fl/fl}$ and *Spry124*$^{-/-}$ MEFs under the indicated conditions.

(legend continued on next page)

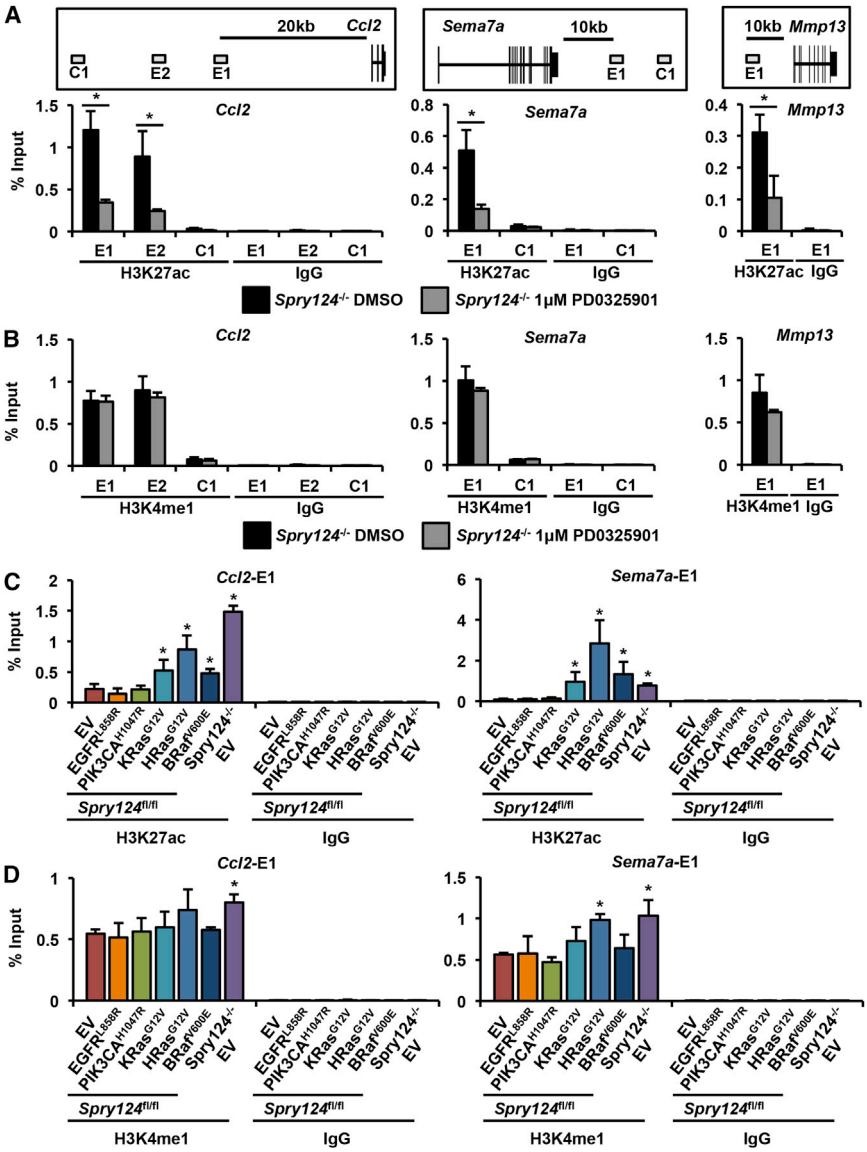

Figure 3. Inhibiting Erk Signaling Decreases H3K27ac at Enhancers, while Oncogenic Activation of the Ras-Raf Axis Promotes H3K27ac at Enhancers

(A and B) ChIP-qPCR for H3K27ac (A) and H3K4me1 (B) at *Ccl2*, *Sema7a*, and *Mmp13* enhancer (labeled E) and control (labeled C) regions upon treatment of *Spry124*$^{-/-}$ MEFs with DMSO or PD0325901. A schematic of primer regions is shown, which correspond to enriched *Spry124*$^{-/-}$ enhancer sites identified using ChIP-seq.

(C and D) ChIP-qPCR for H3K27ac (C) and H3K4me1 (D) at *Ccl2* and *Sema7a* enhancer sites in the indicated MEFs. A schematic of the primer locations is shown in Figure 3A.

n = 3 for (A)–(D). In (A)–(D), the values depict the mean + SD of biological replicates. The p values were calculated by a two-tailed t test; *p < 0.05.

data indicate that aberrant deposition of H3K27ac at enhancers requires persistent Ras-Erk signaling and that BET bromodomain proteins and p300/CBP are necessary for aberrant gene activation upon *Spry* loss.

To test the idea that *Spry* loss would resemble the effects of oncogenes that constitutively activate Ras-ERK and/or PI3K-AKT, we stably transduced *Spry124*$^{fl/fl}$ MEFs with an EV control or a panel of mutant oncogenes (EGFR^{L858R}, PIK3CA^{H1047R}, KRas^{G12V}, HRas^{G12V}, and BRaf^{V600E}) and surveyed the resulting expression and chromatin status of *Spry124*$^{-/-}$ target genes. *Spry124*$^{-/-}$ MEFs transduced with an EV served as a positive control. As expected, these oncogenes modulated Ras-Erk and PI3K-Akt signaling (Figure S3C). KRas^{G12V}, HRas^{G12V}, and BRaf^{V600E} significantly activated all seven *Spry124*$^{-/-}$ target genes tested (Figure S3D). Accordingly, KRas^{G12V}, HRas^{G12V}, and BRaf^{V600E} significantly increased H3K27ac levels at *Spry124*$^{-/-}$ activated enhancers (Figures 3C and S4A). The changes in enhancer marking were largely limited to H3K27ac, as a significant increase in H3K4me1 was only observed at the *Mmp13* enhancer (Figures 3D and S4B). These changes also appeared to be specifically mediated by Ras-Erk signaling. EGFR^{L858R} and PIK3CA^{H1047R}, which preferentially activated Akt, did not stimulate changes in the expression or H3K27ac levels at *Spry124*$^{-/-}$ target genes. These data suggest that, although oncogenic Ras and Raf modulate H3K27ac at shared subsets of *Spry124*$^{-/-}$ enhancers, oncogenes that primarily activate AKT may mediate their effects on cell fate and gene expression through other sets of enhancers.

HRas^{G12V} Transformation Modulates the Enhancer Landscape

To determine the overlap of genes deregulated upon *Spry* loss and those modulated by oncogenes, we performed RNA-seq to identify genes differentially expressed in KRas^{G12V}, HRas^{G12V},

(D) Bar plot of the ratio of TF motif density at gained *Spry124*$^{-/-}$ FGF SEs in the indicated comparison (p < 0.05). Colored bars represent TFs with p < 0.05 and fold change > 1.5. The fold change ranking of select TFs are indicated.

(E) Hierarchical clustering analysis of H3K27ac-defined SE regions in the indicated MEFs. Each biological replicate (rep) is displayed.

(F) UCSC genome browser view of H3K27ac, H3K4me1, and H3K4me3 ChIP-seq binding density at the *Hoxa* cluster in *Spry124*$^{fl/fl}$ and *Spry124*$^{-/-}$ MEFs under the indicated culture conditions. H3K27ac binding density at an adjusted scale is depicted in the box.

n = 2 for (A)–(F). In (A)–(D) and (F), a representative biological replicate is shown. The p values were calculated by a two-tailed t test; *p < 0.05.

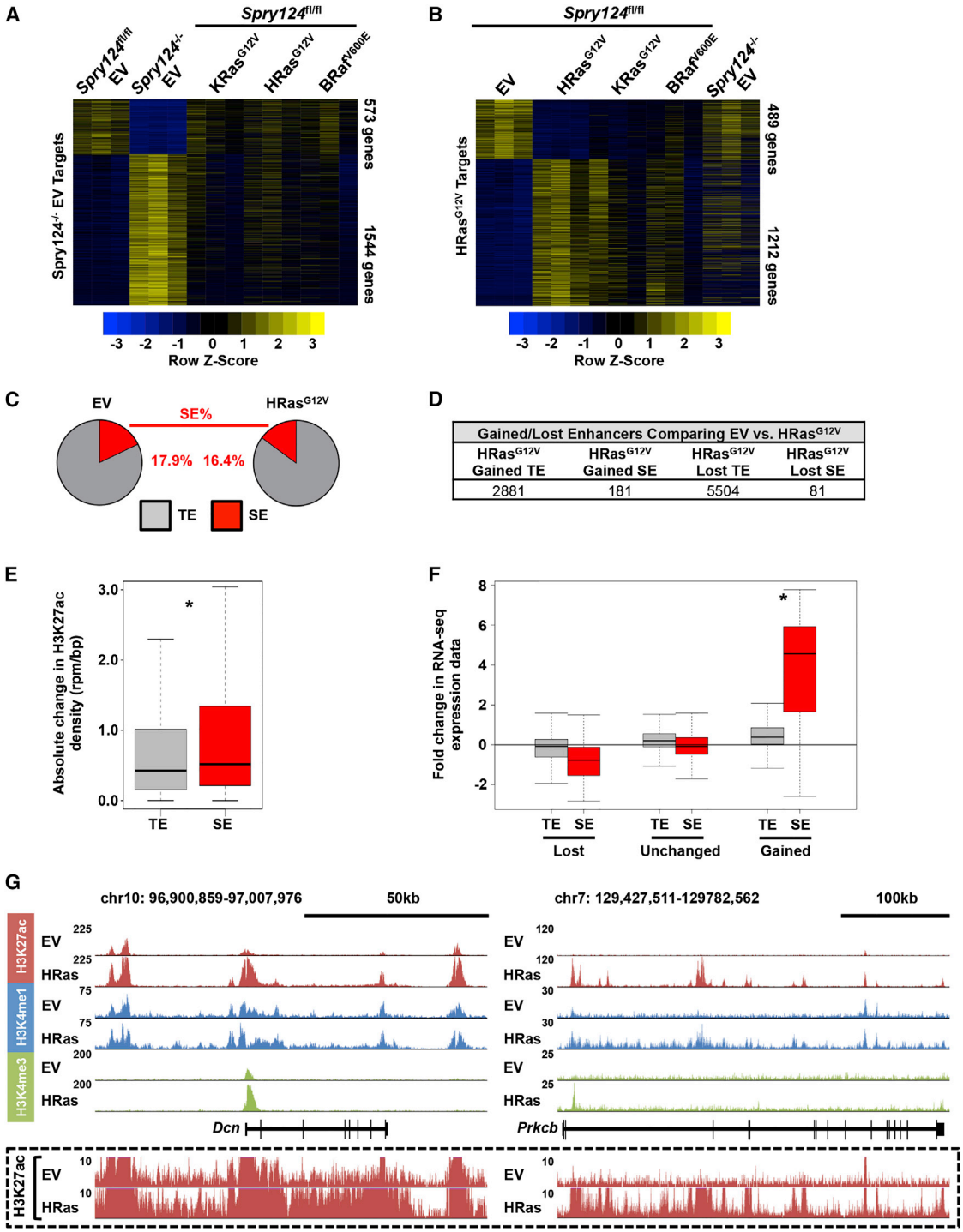

Figure 4. HRas^{G12V} Promotes Global Changes in Chromatin Marking at Enhancers

(A and B) Heatmaps from RNA-seq analyses representing the significantly differentially expressed genes comparing *Spry124*$^{fl/fl}$ EV and *Spry124*$^{-/-}$ EV MEFs (A) or *Spry124*$^{fl/fl}$ EV and HRas^{G12V} MEFs (B).

(C) Pie charts displaying H3K27ac signal at TEs and SEs upon comparison between *Spry124*$^{fl/fl}$ EV and HRas^{G12V} MEFs.

(D) Table summarizing the number of H3K27ac defined enhancers significantly modulated between *Spry124*$^{fl/fl}$ EV and HRas^{G12V} MEFs.

(E) Boxplot of the absolute change in H3K27ac density between *Spry124*$^{fl/fl}$ EV and HRas^{G12V} MEFs at TEs and SEs.

(F) Boxplot of RNA-seq expression for genes proximal to TEs and SEs that were gained, unchanged, or lost in HRas^{G12V} MEFs upon comparison between *Spry124*$^{fl/fl}$ EV and HRas^{G12V} MEFs.

(legend continued on next page)

BRaf^{V600E}, and *Spry124*$^{-/-}$ EV MEFs, compared to *Spry124*$^{fl/fl}$ EV MEFs (Table S2). Surprisingly, the expression pattern of genes modulated in *Spry124*$^{-/-}$ EV MEFs was largely different from those altered by KRas^{G12V}, HRas^{G12V}, or BRaf^{V600E} (Figure 4A). There was a high degree of overlap of genes deregulated in response to KRas^{G12V}, HRas^{G12V}, and BRaf^{V600E} (for example, KRas^{G12V} targets overlapped with 94% of HRas^{G12V} and 59% of BRaf^{V600E} targets), with each of these gene sets having relatively small overlap with *Spry124*$^{-/-}$ EV target genes (*Spry124*$^{-/-}$ EV targets overlapped with 23% of KRas^{G12V}, 34% of HRas^{G12V}, and 19% of BRaf^{V600E} targets) (Figure 4B; Table S2). We noted a core set of 290 deregulated target genes that overlapped in all datasets, which include the validated *Spry124*$^{-/-}$ target genes (Figure S4C). However, IPA revealed that many of the same top classes of genes, such as cancer-associated genes, and pathways, such as cellular movement and proliferation, were shared among the oncogenic Ras, Raf, and *Spry124*$^{-/-}$ gene sets (Figure S4D). This suggests that despite the differences in target genes affected, all four lesions affected common core processes.

The differences in gene expression patterns upon *Spry* loss and oncogene gain, led us to investigate the genome-wide consequences of oncogenic mutations of the Ras-Raf axis on enhancer marking. We performed ChIP-seq for H3K27ac, H3K4me1, and H3K4me3, comparing *Spry124*$^{fl/fl}$ EV and HRas^{G12V} MEFs due to the potent effect of this oncogene on gene expression and H3K27ac at *Spry124*$^{-/-}$ activated enhancers (Figures 3C and S3D). Comparison of *Spry124*$^{fl/fl}$ EV and HRas^{G12V} MEFs revealed that HRas^{G12V} transformation significantly remodeled SEs and TEs (Figures 4C, 4D, S4E, and S4F; Table S5). Consistent with ChIP-qPCR, HRas^{G12V} transformation modified TEs of shared *Spry124*$^{-/-}$ target genes including *Sema7a* (Figures 3C and S5A). However, the absolute change in H3K27ac signal between *Spry124*$^{fl/fl}$ EV and HRas^{G12V} MEFs was significantly greater at SEs than TEs (Figure 4E). Furthermore, genes that gained SEs upon HRas^{G12V} transformation had significantly increased expression levels, compared to genes that gained only TEs (Figure 4F). This result suggests that chromatin changes at SEs generated changes in gene expression upon HRas^{G12V} transformation. For example, HRas^{G12V} transformation resulted in significantly elevated H3K27ac levels at regions associated with the proteoglycan *Dcn*, the glycolate oxidase *Hao1*, and the kinase *Prkcb*, correlating with their elevated expression levels (Figures 4G, S5B, and S7A). We selected these factors as a representative set of HRas^{G12V} target genes with deregulated SEs for further assessment, and we focused on the SE signatures in the subsequent analyses. Collectively, these data demonstrate that HRas^{G12V} globally remodels enhancer marking.

Next, we compared SEs remodeled upon *Spry* loss and HRas^{G12V} transformation, as well as the TF networks deployed by these lesions. Hierarchical clustering analyses revealed that the HRas^{G12V} SE signature was distinct from the *Spry124*$^{fl/fl}$ EV, *Spry124*$^{fl/fl}$, and *Spry124*$^{-/-}$ SE signatures, with only small subsets of SEs found in common (Figure 2E). By examining the SE sequences in these cell lines, we identified the top core regulatory TF network that is likely to bind and activate gene expression in each dataset (Figure 5A). ETS1 was identified as a core TF in both the *Spry124*$^{-/-}$ FGF and HRas^{G12V} networks, consistent with the role of ETS factors as mediators of Ras-ERK signaling (Charlot et al., 2010). However, there were significant differences in the TF networks upon *Spry* loss or HRas^{G12V} transformation. For example, NF-κB1 and MEF2A were identified as core *Spry124*$^{-/-}$ FGF TFs, while GATA4 and MEIS2 were identified as core HRas^{G12V} TFs. We also observed significant differences in TF binding sites enriched at activated SEs upon comparison of *Spry124*$^{-/-}$ FGF and HRas^{G12V} MEFs (Figure 5B; Table S6). In particular, we observed enrichment of binding sites for ARNT ($p < 0.01$) and GATA4 ($p < 0.001$) upon HRas^{G12V} transformation, while binding sites for HOXA1-3 ($p < 0.0001$) were overrepresented upon *Spry* loss. To potentially explain the differences in gene expression upon *Spry* loss and HRas^{G12V} transformation, we examined the levels of phosphotyrosine species in these cells. *Spry124*$^{-/-}$ EV MEFs displayed increased baseline intensity of a ~60-kDa band and a unique ~150- to 185-kDa FGF-induced band (Figure S5C). The larger band may represent phosphorylated FGFR, indicating that *Spry* loss may impact receptor activation at levels above Ras. There were also differences in the intensity of activated Erk and Akt in *Spry124*$^{-/-}$ EV MEFs (Figure S3C). Collectively, our data suggest that differences in the expression profiles and SE signatures upon *Spry* loss and HRas^{G12V} transformation may be due to quantitative and qualitative changes in the activated signaling molecules leading to modulation of different TF networks.

Gata4 Is Required for H3K27ac Marking at Enhancers

To identify TFs responsible for the expression and SE signatures upon HRas^{G12V} transformation, we identified TF binding sites enriched at activated HRas^{G12V} SEs (Figure 6A; Table S6). Significant enrichment of binding sites for TFs such as TWIST1 ($p < 0.01$) was detected upon HRas^{G12V} transformation, consistent with the known role of oncogenic Ras in regulating and cooperating with Twist1 in oncogenesis (De Craene and Berx, 2013). We also noted significant enrichment of binding sites for GATA4 ($p < 0.001$) and identified GATA4 as a core HRas^{G12V} TF (Figures 5A and 6A; Table S6). Furthermore, in HRas^{G12V} MEFs, we observed elevated *Gata4* expression and a marked increase in H3K27ac at a broad TE upstream of *Gata4*, indicating that Gata4 may mediate the oncogenic Ras program (Figures 6B and S7A). *Gata4*, which was not expressed to any significant level in *Spry124*$^{fl/fl}$ MEFs, encodes a TF required for heart development, and *Gata4* mutations cause cardiac dysfunction (Garg et al., 2003). Gata4 knockdown significantly reduced the expression of all four HRas^{G12V} target genes and six out of seven *Spry124*$^{-/-}$ target genes tested (Figures 6C and S6A). Gata4 knockdown led to a significant reduction in H3K27ac, but not H3K4me1, at

(G) UCSC genome browser view of H3K27ac, H3K4me1, and H3K4me3 ChIP-seq binding density at the *Dcn* (left) and *Prkcb* (right) loci in *Spry124*$^{fl/fl}$ EV and HRas^{G12V} MEFs. H3K27ac binding density at an adjusted scale is depicted in the box.

n = 3 for (A) and (B); n = 2 for (C)–(G). In (A) and (B), each biological replicate is shown. In (C)–(G), a representative biological replicate is shown. The p values were calculated by a two-tailed t test; *$p < 0.05$.

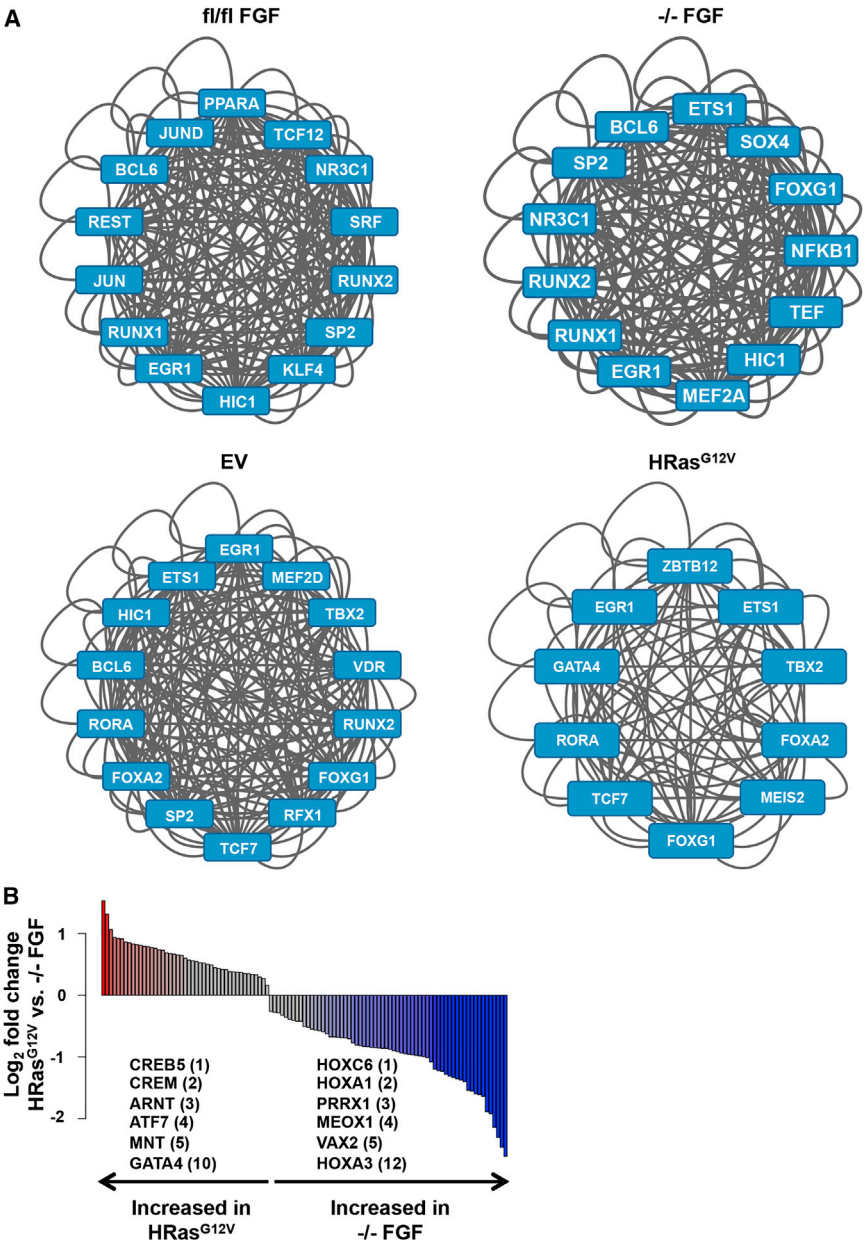

Figure 5. *Spry* Loss and Oncogenic HRas^{G12V} Modify Distinct TF Networks

(A) The top-ranking regulatory TF network identified at SEs in *Spry124*$^{fl/fl}$ FGF, *Spry124*$^{-/-}$ FGF, *Spry124*$^{fl/fl}$ EV, and *Spry124*$^{fl/fl}$ HRas^{G12V} MEFs. Each TF depicted represents a node in the network.

(B) Bar plot of the ratio of TF motif density at gained HRas^{G12V} SEs in the indicated comparison ($p < 0.05$). Colored bars represent TFs with $p < 0.05$ and fold change > 1.5. The fold change ranking of select TFs are indicated.

n = 2 for (A) and (B). In (A) and (B), a representative biological replicate is shown.

HRas^{G12V} Enhancer Signature Identifies *Prkcb* as a Key Downstream Target Gene

The enhancer dysfunction due to HRas^{G12V} transformation led us to investigate whether chemical inhibition of chromatin regulators or target genes with aberrantly marked enhancers could relieve the oncogenic effects of Ras. Consistent with our observations in *Spry124*$^{-/-}$ MEFs, treatment of HRas^{G12V} MEFs with PD0325901 or JQ1 significantly reduced the expression of all four HRas^{G12V} and all seven *Spry124*$^{-/-}$ target genes tested to *Spry124*$^{fl/fl}$ EV levels, indicating their dependence on Erk signaling and BET bromodomain activity (Figure S7A). Accordingly, JQ1 treatment significantly diminished the clonogenicity of HRas^{G12V} MEFs (Figure S7B). JQ1 treatment reduced the viability of HRas^{G12V} MEFs, although *Spry124*$^{fl/fl}$ EV MEFs were also sensitive to inhibition by JQ1 alone. However, a moderate synergistic effect was observed in HRas^{G12V} MEFs upon co-treatment of PD0325901 and JQ1 at doses of 0.1–0.5 μM (Figure S7C). C646 treatment alone also significantly reduced the viability of HRas^{G12V} MEFs, while combinations of C646 and PD0325901 did not reveal a synergistic effect on cell viability (Figure S7D). Our data indicate that BET bromodomain proteins are necessary for the aberrant gene expression, clonogenicity, and viability HRas^{G12V}-transformed cells.

Finally, we explored whether enhancer signatures might reveal dependencies of HRas^{G12V}-transformed cells. In particular, the *Prkcb* locus had dramatically elevated H3K27ac levels upon HRas^{G12V} transformation, correlating with significant overexpression (Figures 4G and S7A). *Prkcb* is frequently amplified in many malignancies and encodes a kinase that is considered a potential therapeutic target in cancer, diabetes, and heart disease (Mochly-Rosen et al., 2012). We hypothesized that

enhancers (Figures 6D, 6E, and S6B). Consistent with the known role of Gata4 as a pioneer factor at enhancers (Cirillo et al., 2002), our data indicate that Gata4 is necessary for maintaining the aberrant H3K27ac marking and gene expression upon HRas^{G12V} transformation. Although Stat3 binding sites were not enriched at activated HRas^{G12V} SEs, a Stat3 expression signature was detected in the HRas^{G12V} RNA-seq datasets (Figure S6C). Stat3 knockdown significantly reduced the expression of all four HRas^{G12V} target genes and six out of seven *Spry124*$^{-/-}$ target genes tested, indicating that Stat3 is also required for aberrant gene activation (Figures S6D and S6E). Together, our data indicate that HRas^{G12V}-driven modulation of H3K27ac at enhancers is dependent on Gata4 and Stat3.

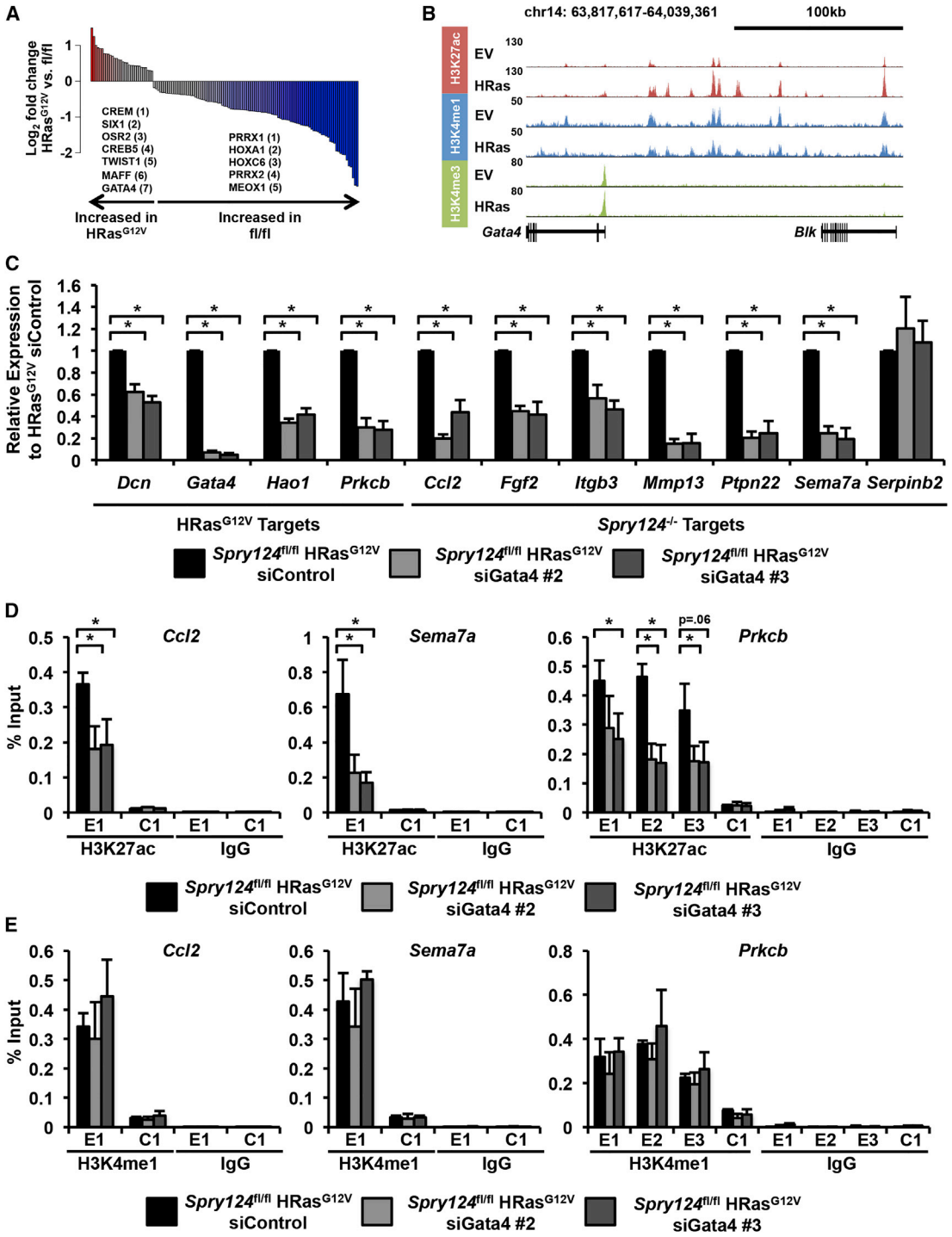

Figure 6. Gata4 Is Required for HRas^{G12V} Expression Programs and H3K27ac Marking at Enhancers

(A) Bar plot of the ratio of TF motif density at gained HRas^{G12V} SEs in the indicated comparison ($p < 0.05$). Colored bars represent TFs with $p < 0.05$ and fold change > 1.5. The fold change ranking of select TFs are indicated.

(B) UCSC genome browser view of H3K27ac, H3K4me1, and H3K4me3 ChIP-seq binding density at the *Gata4* locus in *Spry124*$^{fl/fl}$ EV and HRas^{G12V} MEFs.

(C) Relative mRNA levels of HRas^{G12V} and *Spry124*$^{-/-}$ target genes upon treatment of HRas^{G12V} MEFs with control or *Gata4* siRNAs.

(D and E) ChIP-qPCR for H3K27ac (D) and H3K4me1 (E) at *Ccl2*, *Sema7a*, and *Prkcb* enhancer (labeled E) and control (labeled C) regions upon treatment of HRas^{G12V} MEFs with control or *Gata4* siRNAs. A schematic of the primer locations is shown in Figures 3A and S6B.

n = 2 for (A) and (B); n = 3 for (C)–(E). In (A) and (B), a representative biological replicate is shown. In (C)–(E), the values depict the mean + SD of biological replicates. The p values were calculated by a two-tailed t test; *$p < 0.05$.

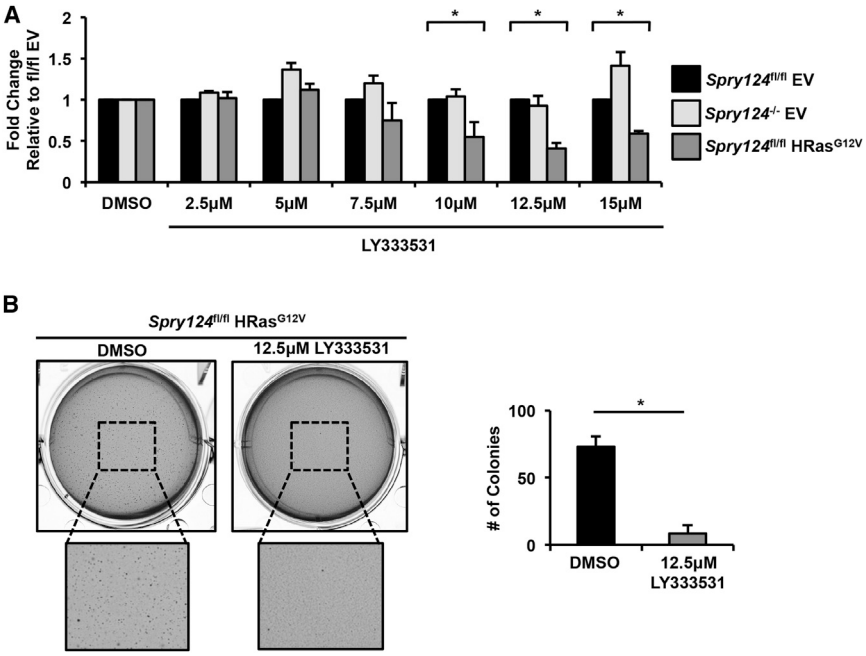

Figure 7. HRas^{G12V}-Transformed Cells Are Sensitive to Prkcb Inhibition

(A) Viability of *Spry124*$^{fl/fl}$ EV, *Spry124*$^{fl/fl}$ HRas^{G12V}, and *Spry124*$^{-/-}$ EV MEFs treated with DMSO or LY333531.

(B) Colony formation analysis of HRas^{G12V} MEFs treated with DMSO or LY333531.

n = 3 for (A) and (B). In (A), the values depict the mean + SD of biological replicates. In (B), a representative well is shown and quantification represents counts per field from mean + SD of biological replicates. The p values were calculated by a two-tailed t test; *p < 0.05 and fold change > 1.5 (A); *p < 0.05 (B).

HRas^{G12V} MEFs would be more sensitive to LY333531, a clinically relevant Prkcb inhibitor also known as ruboxistaurin (Jirousek et al., 1996), than cell lines lacking H3K27ac at the *Prkcb* locus. Indeed, HRas^{G12V} MEFs were significantly more sensitive to doses of LY333531 ranging from 10–15 μM, compared to *Spry124*$^{fl/fl}$ EV or *Spry124*$^{-/-}$ EV MEFs (Figures 7A and S7E). Furthermore, LY333531 treatment significantly reduced the clonogenicity of HRas^{G12V} MEFs (Figure 7B). Collectively, these data highlight that enhancer signatures can aid in the identification of key deregulated chromatin regulators and target genes that are contributing to the oncogenic phenotypes of HRas^{G12V}-transformed cells.

DISCUSSION

Epigenetic deregulation and aberrant activation of RTK signaling pathways drives tumorigenesis. However, the relationship between unrestrained RTK signaling and chromatin modifications at *cis*-regulatory elements remains to be fully elucidated. In this study, we contrasted the effects of loss of feedback regulation and oncogenic RTK signaling on changes in gene expression and enhancer-associated chromatin modifications. We found that *Spry* loss led to Erk-dependent changes in gene expression and H3K27ac deposition at enhancers of genes with key roles in oncogenesis such as the *Hoxa* cluster and *Ccl2*. We and others previously showed that *Spry* loss alters developmental processes such as branching morphogenesis of organs in response to RTK signaling (Basson et al., 2005; Edwin et al., 2009). Furthermore, decreased *Spry* expression, particularly *Spry1* and *Spry2*, has been documented in many malignancies, suggesting that it may play a role in pathogenesis by removing restraints on RTK signaling (Masoumi-Moghaddam et al., 2014). Our data suggest that *Spry* loss and persistent Erk signaling reprograms enhancer-associated chromatin modifications to deregulate gene expression.

Using *Spry*-deficient cells, we aimed to identify general mechanisms relevant to oncogenic Ras- and Raf-driven cancers. Indeed, expression of KRas^{G12V}, HRas^{G12V}, and BRaf^{V600E} led to aberrant activation and H3K27ac marking at a subset of *Spry124*$^{-/-}$ targets. Early work showed that HRas^{G12V} induces a more relaxed chromatin conformation (Laitinen et al., 1990), which is consistent with the increased H3K27ac at enhancers that we observed in response to oncogenic Ras and Raf. However, our study revealed that the majority of deregulated target genes, reprogrammed SEs, and deployed TF networks altered upon HRas^{G12V} transformation are distinct from those modulated upon *Spry* loss. This disparity may result from differences in the strength and duration of Ras-Erk activation in response to these perturbations. Alternatively, RTK and non-RTK pathways may be differentially activated in the contexts of *Spry* loss and HRas^{G12V} transformation. In accordance with the latter idea, we detected a unique FGF-induced ~150- to 185-kDa phosphotyrosine species in *Spry*-deficient cells, which may reflect hyperactivation of the FGFR upon *Spry* loss. Spry proteins limit signaling at many points downstream of the RTK pathway, including the activation of Ras and Raf (Edwin et al., 2009), which may influence the resulting output of chromatin deregulation and aberrant gene expression. Oncogenic EGFR^{L858R} and PIK3CA^{H1047R} potently activated Akt but did not induce changes in the expression or chromatin marking at enhancers of *Spry124*$^{-/-}$ target genes, suggesting that EGFR^{L858R} and PIK3CA^{H1047R} regulate distinct subsets of genes and enhancers. It remains to be determined if aberrant PI3K-AKT signaling results in global chromatin changes, or whether our observations are specific to the Ras-ERK axis.

Due to the high frequency of *RAS* mutations in almost all forms of cancer and the lack of therapies targeting cancers driven by oncogenic Ras, the study of this oncogene has become a centerpiece of new basic and translational research efforts (Stephen et al., 2014). Tumors commonly harbor mutations in both RTK pathway components and chromatin regulators, and recent studies indicate that oncogenic Ras signaling mediated by loss of *Nf1* cooperates with disruption chromatin regulators, including *Mll3* and *Suz12*, to accelerate oncogenesis (Chen

et al., 2014; De Raedt et al., 2014; Kandoth et al., 2013). The BET bromodomain inhibitor JQ1 is highly efficacious in treating preclinical cancer models driven by aberrant Ras activation, including non-small cell lung cancer, acute myeloid leukemia, and malignant peripheral nerve sheath tumors (Chen et al., 2014; De Raedt et al., 2014; Shimamura et al., 2013). In accordance with these studies, we found that JQ1 treatment repressed the aberrant transcriptional responses and clonogenicity of $HRas^{G12V}$-transformed cells. In viability assays, control cells were more sensitive to JQ1 treatment than $HRas^{G12V}$-transformed cells, which may be due to the high level of amplified RTK signaling and redistribution of H3K27ac at key target genes upon $HRas^{G12V}$ transformation. Combining low doses of PD0325901 with JQ1 was moderately more potent than using each compound alone in $HRas^{G12V}$-transformed cells. The lack of a more potent effect when combining these compounds may be due to their convergence on a shared set of target genes or their sharp dose-response curves, such that suboptimal doses of the drugs fail to effectively inhibit gene expression. Investigation into the functional role of BET bromodomain proteins in oncogenic Ras-driven cancers will provide further insight into the mechanisms driving oncogenesis.

H3K27ac enhancer signatures are useful in the identification of aberrant oncogenic transcriptional programs and classification of malignant tissue (Chapuy et al., 2013). $HRas^{G12V}$ SE signatures and TF motif analyses highlighted Gata4 as a candidate TF promoting the oncogenic $HRas^{G12V}$ program. We demonstrate that Gata4 is required for the aberrant H3K27ac enhancer marking and expression changes upon $HRas^{G12V}$ transformation. Previous studies showed that Gata4 is regulated by post-translational modifications, including phosphorylation by kinases downstream of ERK (Liang et al., 2001). Our data suggest that Gata4 may be a misregulated pioneer factor downstream of oncogenic $HRas^{G12V}$, activated through a feed-forward loop due to aberrant enhancer marking. We also identified Prkcb as an $HRas^{G12V}$ target susceptible to chemical inhibition, which promotes the viability and clonogenicity of $HRas^{G12V}$-transformed cells. One limitation of our study is that the experiments were performed exclusively in MEFs. Therefore, further work will be required to evaluate the functional role of Gata4 and clinical significance of BET bromodomain and Prkcb inhibition in oncogenic Ras-driven epithelial cancers using appropriate cell and mouse models. In sum, our study shows that examination of histone modification signatures and identification of oncogene-regulated enhancers can yield insight into the key processes and targets that drive malignancy. Our data support a model in which unrestrained RTK signaling modulates gene expression through coordinated regulation of enhancers.

EXPERIMENTAL PROCEDURES

Cell Lines, Culture Conditions, and FGF Treatment

Spry124$^{fl/fl}$ and *Spry124*$^{-/-}$ MEFs were cultured in DMEM containing 10% fetal bovine serum (FBS) as previously described (Akbulut et al., 2010). Unsynchronized MEFs were maintained in DMEM containing 10% FBS for 24 hr. Serum-starved MEFs were maintained in DMEM containing 0.1% FBS for 24 hr. FGF-treated MEFs were maintained in DMEM containing 0.1% FBS for 20 hr, after which 10 ng/ml FGF (Life Technologies) was directly added to the media for an additional 4 hr, unless otherwise noted. Additional details related to retroviral transduction, inhibitor treatments, small interfering RNA transfection, protein and RNA isolation, and biological assays can be found in the Supplemental Experimental Procedures.

ChIP-qPCR and ChIP-Seq

ChIP experiments for histone modifications were performed as described previously (Martinez-Garcia et al., 2011). ChIP-seq analyses were performed as described previously (Lovén et al., 2013). Antibodies, primers, and detailed ChIP-seq analyses are described in the Supplemental Experimental Procedures.

ACCESSION NUMBER

ChIP-seq and RNA-seq data reported in this paper have been deposited to the NCBI GEO and are available under accession number GEO: GSE64195.

SUPPLEMENTAL INFORMATION

Supplemental Information includes Supplemental Experimental Procedures, seven figures, and six tables and can be found with this article online at http://dx.doi.org/10.1016/j.celrep.2015.06.078.

AUTHOR CONTRIBUTIONS

B.N. and J.D.L. designed the research and interpreted the data. B.N. performed the experiments and received assistance from C.M.W., R.P., and T.E. P.Ó., K.S., and A.A.G. performed the RNA-seq analyses and contributed to the ChIP-seq analyses. J.M.R., C.Y.L., and J.E.B. performed the ChIP-seq analyses. B.N. and J.D.L. wrote the manuscript.

ACKNOWLEDGMENTS

This work was initiated under grants from the NIH (CA59998) and the Lynn Sage and Northwestern Memorial Foundations and supported by a NCI Physical Sciences-Oncology Center grant (U54CA143869 to J.D.L.). This work was also supported by an NIH T32 training grant (GM08061 to B.N.), a Northwestern University Malkin Scholars Award (B.N.), an NIGMS T32 training grant (GM007288 to K.S.), and a Department of Defense CDMRP (CA120184 to C.Y.L.). We thank members of the J.D.L. laboratory and Suzanne Nabet for helpful discussions and critical review of the manuscript.

Received: December 29, 2014
Revised: May 11, 2015
Accepted: June 23, 2015
Published: August 13, 2015

REFERENCES

Agger, K., Cloos, P.A., Rudkjaer, L., Williams, K., Andersen, G., Christensen, J., and Helin, K. (2009). The H3K27me3 demethylase JMJD3 contributes to the activation of the INK4A-ARF locus in response to oncogene- and stress-induced senescence. Genes Dev. *23*, 1171–1176.

Akbulut, S., Reddi, A.L., Aggarwal, P., Ambardekar, C., Canciani, B., Kim, M.K., Hix, L., Vilimas, T., Mason, J., Basson, M.A., et al. (2010). Sprouty proteins inhibit receptor-mediated activation of phosphatidylinositol-specific phospholipase C. Mol. Biol. Cell *21*, 3487–3496.

Barradas, M., Anderton, E., Acosta, J.C., Li, S., Banito, A., Rodriguez-Niedenführ, M., Maertens, G., Banck, M., Zhou, M.M., Walsh, M.J., et al. (2009). Histone demethylase JMJD3 contributes to epigenetic control of INK4a/ARF by oncogenic RAS. Genes Dev. *23*, 1177–1182.

Barrett, S.D., Bridges, A.J., Dudley, D.T., Saltiel, A.R., Fergus, J.H., Flamme, C.M., Delaney, A.M., Kaufman, M., LePage, S., Leopold, W.R., et al. (2008). The discovery of the benzhydroxamate MEK inhibitors CI-1040 and PD 0325901. Bioorg. Med. Chem. Lett. *18*, 6501–6504.

Basson, M.A., Akbulut, S., Watson-Johnson, J., Simon, R., Carroll, T.J., Shakya, R., Gross, I., Martin, G.R., Lufkin, T., McMahon, A.P., et al. (2005). Sprouty1 is a critical regulator of GDNF/RET-mediated kidney induction. Dev. Cell *8*, 229–239.

Bowers, E.M., Yan, G., Mukherjee, C., Orry, A., Wang, L., Holbert, M.A., Crump, N.T., Hazzalin, C.A., Liszczak, G., Yuan, H., et al. (2010). Virtual ligand screening of the p300/CBP histone acetyltransferase: identification of a selective small molecule inhibitor. Chem. Biol. *17*, 471–482.

Brown, J.D., Lin, C.Y., Duan, Q., Griffin, G., Federation, A.J., Paranal, R.M., Bair, S., Newton, G., Lichtman, A.H., Kung, A.L., et al. (2014). NF-κB directs dynamic super enhancer formation in inflammation and atherogenesis. Mol. Cell *56*, 219–231.

Chapuy, B., McKeown, M.R., Lin, C.Y., Monti, S., Roemer, M.G., Qi, J., Rahl, P.B., Sun, H.H., Yeda, K.T., Doench, J.G., et al. (2013). Discovery and characterization of super-enhancer-associated dependencies in diffuse large B cell lymphoma. Cancer Cell *24*, 777–790.

Charlot, C., Dubois-Pot, H., Serchov, T., Tourrette, Y., and Wasylyk, B. (2010). A review of post-translational modifications and subcellular localization of Ets transcription factors: possible connection with cancer and involvement in the hypoxic response. Methods Mol. Biol. *647*, 3–30.

Chen, Y.J., Wang, Y.N., and Chang, W.C. (2007). ERK2-mediated C-terminal serine phosphorylation of p300 is vital to the regulation of epidermal growth factor-induced keratin 16 gene expression. J. Biol. Chem. *282*, 27215–27228.

Chen, C., Liu, Y., Rappaport, A.R., Kitzing, T., Schultz, N., Zhao, Z., Shroff, A.S., Dickins, R.A., Vakoc, C.R., Bradner, J.E., et al. (2014). MLL3 is a haploinsufficient 7q tumor suppressor in acute myeloid leukemia. Cancer Cell *25*, 652–665.

Cirillo, L.A., Lin, F.R., Cuesta, I., Friedman, D., Jarnik, M., and Zaret, K.S. (2002). Opening of compacted chromatin by early developmental transcription factors HNF3 (FoxA) and GATA-4. Mol. Cell *9*, 279–289.

Creyghton, M.P., Cheng, A.W., Welstead, G.G., Kooistra, T., Carey, B.W., Steine, E.J., Hanna, J., Lodato, M.A., Frampton, G.M., Sharp, P.A., et al. (2010). Histone H3K27ac separates active from poised enhancers and predicts developmental state. Proc. Natl. Acad. Sci. USA *107*, 21931–21936.

De Craene, B., and Berx, G. (2013). Regulatory networks defining EMT during cancer initiation and progression. Nat. Rev. Cancer *13*, 97–110.

De Raedt, T., Beert, E., Pasmant, E., Luscan, A., Brems, H., Ortonne, N., Helin, K., Hornick, J.L., Mautner, V., Kehrer-Sawatzki, H., et al. (2014). PRC2 loss amplifies Ras-driven transcription and confers sensitivity to BRD4-based therapies. Nature *514*, 247–251.

Edwin, F., Anderson, K., Ying, C., and Patel, T.B. (2009). Intermolecular interactions of Sprouty proteins and their implications in development and disease. Mol. Pharmacol. *76*, 679–691.

Filippakopoulos, P., Qi, J., Picaud, S., Shen, Y., Smith, W.B., Fedorov, O., Morse, E.M., Keates, T., Hickman, T.T., Felletar, I., et al. (2010). Selective inhibition of BET bromodomains. Nature *468*, 1067–1073.

Garg, V., Kathiriya, I.S., Barnes, R., Schluterman, M.K., King, I.N., Butler, C.A., Rothrock, C.R., Eapen, R.S., Hirayama-Yamada, K., Joo, K., et al. (2003). GATA4 mutations cause human congenital heart defects and reveal an interaction with TBX5. Nature *424*, 443–447.

Göke, J., Chan, Y.S., Yan, J., Vingron, M., and Ng, H.H. (2013). Genome-wide kinase-chromatin interactions reveal the regulatory network of ERK signaling in human embryonic stem cells. Mol. Cell *50*, 844–855.

Hacohen, N., Kramer, S., Sutherland, D., Hiromi, Y., and Krasnow, M.A. (1998). sprouty encodes a novel antagonist of FGF signaling that patterns apical branching of the Drosophila airways. Cell *92*, 253–263.

Heintzman, N.D., Stuart, R.K., Hon, G., Fu, Y., Ching, C.W., Hawkins, R.D., Barrera, L.O., Van Calcar, S., Qu, C., Ching, K.A., et al. (2007). Distinct and predictive chromatin signatures of transcriptional promoters and enhancers in the human genome. Nat. Genet. *39*, 311–318.

Herz, H.M., Mohan, M., Garruss, A.S., Liang, K., Takahashi, Y.H., Mickey, K., Voets, O., Verrijzer, C.P., and Shilatifard, A. (2012). Enhancer-associated H3K4 monomethylation by Trithorax-related, the Drosophila homolog of mammalian Mll3/Mll4. Genes Dev. *26*, 2604–2620.

Hu, S., Xie, Z., Onishi, A., Yu, X., Jiang, L., Lin, J., Rho, H.S., Woodard, C., Wang, H., Jeong, J.S., et al. (2009). Profiling the human protein-DNA interactome reveals ERK2 as a transcriptional repressor of interferon signaling. Cell *139*, 610–622.

Jirousek, M.R., Gillig, J.R., Gonzalez, C.M., Heath, W.F., McDonald, J.H., 3rd, Neel, D.A., Rito, C.J., Singh, U., Stramm, L.E., Melikian-Badalian, A., et al. (1996). (S)-13-[(dimethylamino)methyl]-10,11,14,15-tetrahydro-4,9:16,21-dimetheno-1H, 13H-dibenzo[e,k]pyrrolo[3,4-h][1,4,13]oxadiazacyclohexadecene-1,3(2H)-d ione (LY333531) and related analogues: isozyme selective inhibitors of protein kinase C beta. J. Med. Chem. *39*, 2664–2671.

Kaikkonen, M.U., Spann, N.J., Heinz, S., Romanoski, C.E., Allison, K.A., Stender, J.D., Chun, H.B., Tough, D.F., Prinjha, R.K., Benner, C., and Glass, C.K. (2013). Remodeling of the enhancer landscape during macrophage activation is coupled to enhancer transcription. Mol. Cell *51*, 310–325.

Kandoth, C., McLellan, M.D., Vandin, F., Ye, K., Niu, B., Lu, C., Xie, M., Zhang, Q., McMichael, J.F., Wyczalkowski, M.A., et al. (2013). Mutational landscape and significance across 12 major cancer types. Nature *502*, 333–339.

Laitinen, J., Sistonen, L., Alitalo, K., and Hölttä, E. (1990). c-Ha-rasVal 12 oncogene-transformed NIH-3T3 fibroblasts display more decondensed nucleosomal organization than normal fibroblasts. J. Cell Biol. *111*, 9–17.

Liang, Q., Wiese, R.J., Bueno, O.F., Dai, Y.S., Markham, B.E., and Molkentin, J.D. (2001). The transcription factor GATA4 is activated by extracellular signal-regulated kinase 1- and 2-mediated phosphorylation of serine 105 in cardiomyocytes. Mol. Cell. Biol. *21*, 7460–7469.

Lovén, J., Hoke, H.A., Lin, C.Y., Lau, A., Orlando, D.A., Vakoc, C.R., Bradner, J.E., Lee, T.I., and Young, R.A. (2013). Selective inhibition of tumor oncogenes by disruption of super-enhancers. Cell *153*, 320–334.

Martinez-Garcia, E., Popovic, R., Min, D.J., Sweet, S.M., Thomas, P.M., Zamdborg, L., Heffner, A., Will, C., Lamy, L., Staudt, L.M., et al. (2011). The MMSET histone methyl transferase switches global histone methylation and alters gene expression in t(4;14) multiple myeloma cells. Blood *117*, 211–220.

Masoumi-Moghaddam, S., Amini, A., and Morris, D.L. (2014). The developing story of Sprouty and cancer. Cancer Metastasis Rev. *33*, 695–720.

Mochly-Rosen, D., Das, K., and Grimes, K.V. (2012). Protein kinase C, an elusive therapeutic target? Nat. Rev. Drug Discov. *11*, 937–957.

Ostuni, R., Piccolo, V., Barozzi, I., Polletti, S., Termanini, A., Bonifacio, S., Curina, A., Prosperini, E., Ghisletti, S., and Natoli, G. (2013). Latent enhancers activated by stimulation in differentiated cells. Cell *152*, 157–171.

Rada-Iglesias, A., Bajpai, R., Swigut, T., Brugmann, S.A., Flynn, R.A., and Wysocka, J. (2011). A unique chromatin signature uncovers early developmental enhancers in humans. Nature *470*, 279–283.

Schutzman, J.L., and Martin, G.R. (2012). Sprouty genes function in suppression of prostate tumorigenesis. Proc. Natl. Acad. Sci. USA *109*, 20023–20028.

Shim, K., Minowada, G., Coling, D.E., and Martin, G.R. (2005). Sprouty2, a mouse deafness gene, regulates cell fate decisions in the auditory sensory epithelium by antagonizing FGF signaling. Dev. Cell *8*, 553–564.

Shimamura, T., Chen, Z., Soucheray, M., Carretero, J., Kikuchi, E., Tchaicha, J.H., Gao, Y., Cheng, K.A., Cohoon, T.J., Qi, J., et al. (2013). Efficacy of BET bromodomain inhibition in Kras-mutant non-small cell lung cancer. Clin. Cancer Res. *19*, 6183–6192.

Smith, E., and Shilatifard, A. (2014). Enhancer biology and enhanceropathies. Nat. Struct. Mol. Biol. *21*, 210–219.

Soloaga, A., Thomson, S., Wiggin, G.R., Rampersaud, N., Dyson, M.H., Hazzalin, C.A., Mahadevan, L.C., and Arthur, J.S. (2003). MSK2 and MSK1 mediate the mitogen- and stress-induced phosphorylation of histone H3 and HMG-14. EMBO J. *22*, 2788–2797.

Spitz, F., and Furlong, E.E. (2012). Transcription factors: from enhancer binding to developmental control. Nat. Rev. Genet. *13*, 613–626.

Stephen, A.G., Esposito, D., Bagni, R.K., and McCormick, F. (2014). Dragging ras back in the ring. Cancer Cell *25*, 272–281.

Tee, W.W., Shen, S.S., Oksuz, O., Narendra, V., and Reinberg, D. (2014). Erk1/2 activity promotes chromatin features and RNAPII phosphorylation at developmental promoters in mouse ESCs. Cell *156*, 678–690.

Tie, F., Banerjee, R., Stratton, C.A., Prasad-Sinha, J., Stepanik, V., Zlobin, A., Diaz, M.O., Scacheri, P.C., and Harte, P.J. (2009). CBP-mediated acetylation of histone H3 lysine 27 antagonizes Drosophila Polycomb silencing. Development *136*, 3131–3141.

Turner, N., and Grose, R. (2010). Fibroblast growth factor signalling: from development to cancer. Nat. Rev. Cancer *10*, 116–129.

Whyte, W.A., Orlando, D.A., Hnisz, D., Abraham, B.J., Lin, C.Y., Kagey, M.H., Rahl, P.B., Lee, T.I., and Young, R.A. (2013). Master transcription factors and mediator establish super-enhancers at key cell identity genes. Cell *153*, 307–319.

Yu, H., Pardoll, D., and Jove, R. (2009). STATs in cancer inflammation and immunity: a leading role for STAT3. Nat. Rev. Cancer *9*, 798–809.